

## Programmable ion-sensitive transistor interfaces. III. Design considerations, signal generation, and sensitivity enhancement

Krishna Jayant,<sup>1,\*</sup> Kshitij Auluck,<sup>1</sup> Sergio Rodriguez,<sup>2</sup> Yingqiu Cao,<sup>1</sup> and Edwin C. Kan<sup>1</sup>

<sup>1</sup>*Electrical and Computer Engineering, Cornell University, Ithaca, New York 14853, USA*

<sup>2</sup>*Department of Biology, Randolph College, Lynchburg, Virginia 24503, USA*

(Received 5 March 2014; published 30 May 2014)

We report on factors that affect DNA hybridization detection using ion-sensitive field-effect transistors (ISFETs). Signal generation at the interface between the transistor and immobilized biomolecules is widely ascribed to unscreened molecular charges causing a shift in surface potential and hence the transistor output current. Traditionally, the interaction between DNA and the dielectric or metal sensing interface is modeled by treating the molecular layer as a sheet charge and the ionic profile with a Poisson-Boltzmann distribution. The surface potential under this scenario is described by the Grahame equation. This approximation, however, often fails to explain large hybridization signals on the order of tens of mV. More realistic descriptions of the DNA-transistor interface which include factors such as ion permeation, exclusion, and packing constraints have been proposed with little or no corroboration against experimental findings. In this study, we examine such physical models by their assumptions, range of validity, and limitations. We compare simulations against experiments performed on electrolyte-oxide-semiconductor capacitors and foundry-ready floating-gate ISFETs. We find that with weakly charged interfaces (i.e., low intrinsic interface charge), pertinent to the surfaces used in this study, the best agreement between theory and experiment exists when ions are completely excluded from the DNA layer. The influence of various factors such as bulk pH, background salinity, chemical reactivity of surface groups, target molecule concentration, and surface coatings on signal generation is studied. Furthermore, in order to overcome Debye screening limited detection, we suggest two signal enhancement strategies. We first describe frequency domain biosensing, highlighting the ability to sort short DNA strands based on molecular length, and then describe DNA biosensing in multielectrolytes comprising trace amounts of higher-valency salt in a background of monovalent saline. Our study provides guidelines for optimized interface design, signal enhancement, and the interpretation of FET-based biosensor signals.

DOI: [10.1103/PhysRevE.89.052817](https://doi.org/10.1103/PhysRevE.89.052817)

PACS number(s): 73.40.Mr, 82.47.Rs, 68.47.Pe, 87.80.-y

### I. INTRODUCTION

Development of label-free electronic detectors for DNA molecules is central to applications ranging from biosensing, sequencing, and diagnostics. The use of ion-sensitive field-effect transistors (ISFETs) for electrochemical detection of biomolecules [1–6] provides a fast and sensitive signal transducing scheme applicable across a wide range of target concentrations (fM to  $\mu$ M sensitivity) [7,8]. Detection is conventionally sought through direct molecular charge transduction [4]. The commonly accepted notion of signal generation is that intrinsic molecular charges immobilized on the open oxide interface modulate the net surface charge ( $\sigma_O$ ) and set a new equilibrium surface potential ( $\psi_O$ ). In order to theoretically corroborate experimental observations, the updated  $\sigma_O$  and  $\psi_O$  conditions are calculated using the Poisson-Boltzmann (PB) approximation described by the Grahame equation

$$\sigma_O = \sqrt{8\varepsilon_{\text{medium}}kTn_O} \sinh\left(\frac{ze\psi_O}{2kT}\right). \quad (1)$$

Here  $\varepsilon_{\text{medium}}$  is the absolute permittivity of the buffer,  $n_O$  is the electrolyte ion concentration,  $k$  is the Boltzmann constant, and  $T$  is the temperature. The difference in  $\psi_O$  before and after

DNA addition is then

$$\Delta\psi_O = \frac{2kT}{ze} \arcsin h\left(\frac{\sigma_O + \sigma_{\text{DNA}}}{\sqrt{8\varepsilon_{\text{medium}}kTn_O}}\right) - \frac{2kT}{ze} \arcsin h\left(\frac{\sigma_O}{\sqrt{8\varepsilon_{\text{medium}}kTn_O}}\right). \quad (2)$$

This method of signal interpretation assumes that DNA is akin to a sheet charge. The strong nonlinear screening imposed by the PB formulation “mathematically” does not allow  $\psi_O$  to rise too high, especially under high  $\sigma_O$  conditions. Fritz and colleagues [4] corroborated their experimental observations against the standard Grahame equation and showed that an intrinsic surface charge density of  $0.8 \text{ C/m}^2$ , corresponds to a  $\Delta\psi_O$  (i.e., surface potential shifts during hybridization) of 3 mV. While the Grahame equation corroborates the  $\Delta\psi_O$  observed on thermally grown pristine oxides, it fails to account for large  $\Delta\psi_O$  values often encountered in experiments involving nontraditional surfaces [9]. For example,  $\Delta\psi_O$  ranging between 3 mV and 800 mV–1 V [9] have been reported for a variety of interfaces. It is also important to note that DNA is always accompanied by counterions and often forms a layer of finite thickness at the transistor interface. It thus becomes imperative to consider both layer thickness and different screening properties within these molecular layers to validate and predict experimental observations. Recent reports that have considered screening properties within DNA layers attribute the mechanisms of signal generation to either ion exclusion, formation of a Donnan membrane potential, or

\*Corresponding author: [kj75@cornell.edu](mailto:kj75@cornell.edu); FAX: 607/254-3508.

differences in permittivity [10–17] between the DNA and electrolyte phase. Most of these studies have been theoretical in nature with very little experimental corroboration. It is still unclear as to how properties such as the surface  $pH$  response (Nernstian vs non-Nernstian),  $E$ -field dependent surface ionizability, and electrolyte composition affect signal generation within the framework of such membrane models. Two questions that we specifically address are (i) what combination of physical effects accurately explains the large deviation from theory? and (ii) how can optimal sensitivity be established? We first discuss some of the physical effects below.

The first critical aspect to DNA sensing is the nature of the interface and its net intrinsic charge [4]. Studies have shown very low hybridization signals on surfaces exhibiting high intrinsic surface charge, while metal interfaces [9] or weakly charged polysilicon [15] surfaces have revealed large signal shifts of  $\sim 50$ – $100$  mV. A direct comparison under identical conditions would help narrow the differences. Furthermore, the difference is generally attributed to molecular charge screening by surface groups. However, surface groups are ionized as a function of  $pH$  and electric field [18]. So this raises the question, if DNA is charged, should it not shift the surface chemical equilibrium and affect the ionizability of the surface groups?

An important concern that is often raised with FET-based sensing is Debye screening, expressed in Eq. (3). Ionic screening of molecular charges characterized by the Debye length is dependent only on the overall ionic concentration.

$$\lambda_D = \sqrt{\frac{\epsilon_{\text{medium}} k T}{2e^2 z^2 n_O}}. \quad (3)$$

Debye screening lengths ( $\lambda_D$ ) decrease as global saline concentrations increase, thus effectively shielding DNA charges from the transistor surface. In addition to anions and cations, bulk  $pH$  ( $pH_B$ ) can also play an important role with respect to screening [19,20]. Recently it was shown that as  $pH_B$  was lowered the DNA packing and hybridization efficiency increased, thereby increasing the deflection of a nanomechanical beam [21]. This was an important result as it implied that by lowering  $pH_B$  interstrand repulsion could be lowered which resulted in an increase in hybridization efficiency. Furthermore,  $pH_B$  can also tune the net surface charge and hence  $\psi_O$  [18]. Such a change in  $\psi_O$  can affect DNA binding, surface ion concentration, and molecular orientation [15]. Hence elucidating the role of  $pH_B$  on DNA interactions at the transistor interface is paramount.

A parameter of interest within the screening framework is the role of permittivity within tightly packed molecular layers. Such effects have often been neglected in corroborating experimental data. Studies, however, have shown that there exists a gradient in permittivity which extends from the membrane-electrolyte interface into the bulk [22]. Recently, we showed that in order to match large experimentally observed hybridization signals of  $\sim 50$ – $60$  mV, it was required to account for such permittivity differences [15], since a lowering in molecular layer permittivity would result in pronounced ion exclusion and in turn lower screening. While such a hypothesis agreed with experiment, the validity of such a model across different  $pH_B$  conditions was not established. In this study we further shed light on this particular aspect.

Addition of a surface monolayer (SAM) such as poly-L-lysine (PLL) or (3-aminopropyl)triethoxysilane to chemically functionalize the interface facilitates molecular binding, but can further riddle the observed signal. So far, most studies have focused on molecule orientation and linker chemistries [23]. However, the intrinsic  $pH$  response of the SAM interface is often ignored. As previously mentioned the intrinsic charges on DNA could shift the surface chemical equilibrium and appear as an applied  $E$  field. Hence it becomes important to understand how SAMs affect the intrinsic  $pH$  sensitivity and the conditions under which such effects become non-negligible.

The target concentration also plays an important role in deciding hybridization efficiency [24]. A high target concentration can lead to steric hindrance and repulsion between incoming target strands, and thus hinder the diffusion towards the immobilized probe layer. Such blockage prevents efficient hybridization and can lower the readout signal. In this work, we discuss the implications of adding high target concentrations and also present evidence of how surface heterogeneity can affect binding isotherms [3,11,25].

As salinity,  $pH_B$ , membrane screening, probe and target density, and surface charge all have effects on signal generation and sensitivity, tuning each parameter for optimal signal enhancement becomes daunting. For example, studies have proposed that in order to improve hybridization efficiency one could tune the global saline levels [26], where hybridization is performed in high saline concentrations and readout under low saline conditions. While changing salinity levels between hybridization and readout seems attractive and can be readily achieved with microfluidic integration, a shift in global saline levels can change the buffering response of surface hydroxyl groups [18,27], which can further complicate the interpretation of the recorded signal. Another attractive approach adopted by researchers is the combination of DNA amplification and  $pH$  or ion sensitivity [28,29]. Although these techniques are promising, the use of enzymes for amplification makes it hard for long-term storage and handling of reagents. In order to circumvent such difficulties so that ISFET operation is possible under high saline conditions, we present two alternatives to enhance the recorded signal. The first alternative employs frequency-mode operation which probes the dielectric and resistive properties of the molecular layer, and the second deals with performing hybridization reactions in the presence of trace levels of multivalent salt. With the former we present length sorting of short double-stranded DNA (dsDNA), and with the latter we discuss the implications of DNA condensation [30] and localized screening modulation as a method to improve DNA biosensing.

## II. METHODS

### A. Materials

Electrolyte-oxide-semiconductor (EOS) capacitors and floating-gate ISFETs termed the  $C_V$ MOS were fabricated as described previously [18]. The capacitors were fabricated on  $p$ -type silicon wafers with highly doped polysilicon and  $\text{SiO}_2$  interfaces exposed to the electrolyte. A nitride passivation was added to reduce ion drift. An epoxy reservoir avoids the fluid from reaching the bond pads and provides electrical isolation. The  $C_V$ MOS transistors (Fig. 1) were fabricated in a  $1.5 \mu\text{m}$

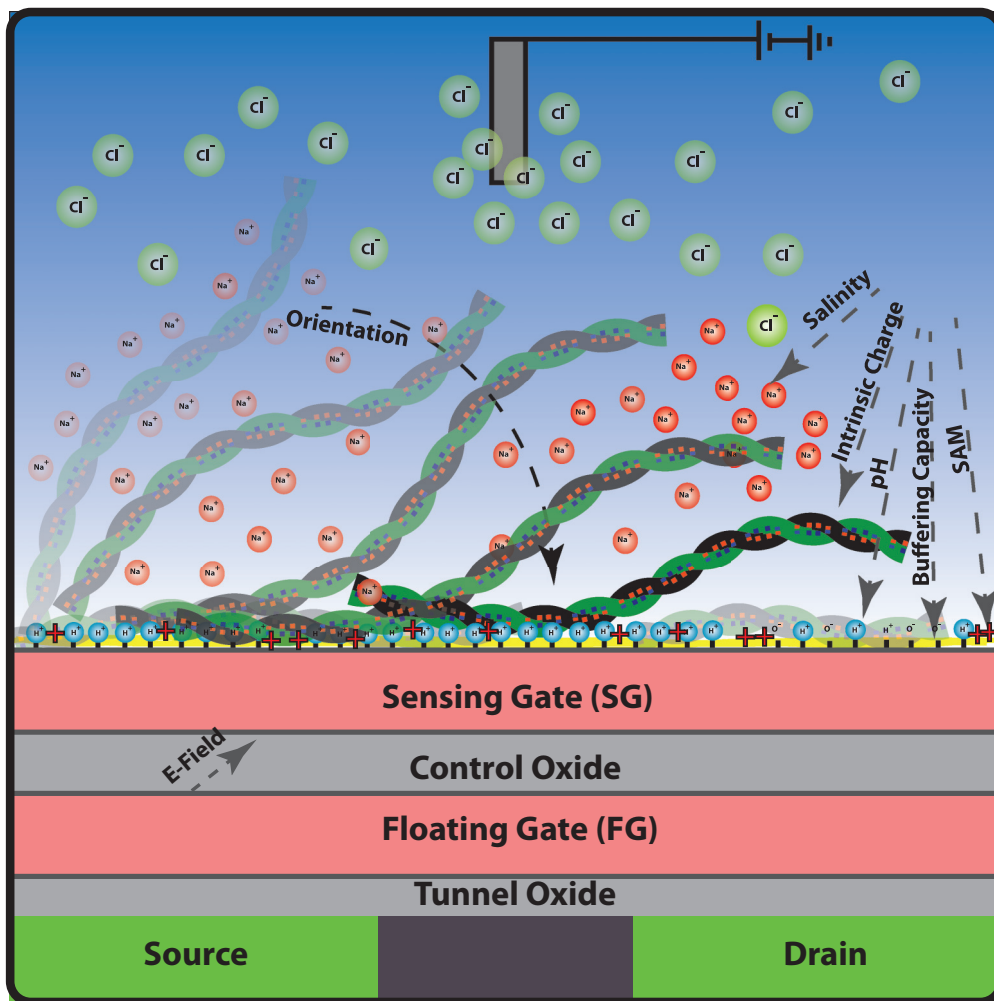


FIG. 1. (Color online) The CVMOS transistor with DNA molecules immobilized on the SG. Various factors that affect signal generation at the SG interface are shown. The  $E$  field in the SG oxide is tuned by either modulating the control gate (not shown) bias or FG charge.

AMI foundry process [18,31]. Briefly, the tunnel oxide refers to the oxide between the channel and the floating gate (FG), while the control oxides represent the oxide between the control and sensing gates (CG and SG) and FG. The FG is electrically floating. The reference electrode pins the electrolyte bulk to ( $V_{ref}$ ), while the CG can be used to program, erase, or bias the device to a desired region of operation. The tunnel and control oxide thicknesses are 10 and 35 nm, respectively. The control gate area is  $25 \mu\text{m} \times 40 \mu\text{m}$ , while sensing gates vary between  $5 \mu\text{m} \times 400 \mu\text{m}$  and  $200 \mu\text{m} \times 400 \mu\text{m}$ . The chip was cleaned with de-ionized (DI) water, isopropyl alcohol and coated with PLL before each test. The chips were subsequently set aside for 2 hours washed with DI water, dried, and stored at  $4^\circ\text{C}$  before use. A small reservoir made of epoxy was similarly created as in the case for EOS capacitors.

Single and complementary strands of DNA of varying lengths [16 (B1,B2), 25 (C1,C2), and 48 bp (D1,D2)] (see Table I) were procured from IDT DNA and 99.9% HPLC (High-performance liquid chromatography purified). DNA was maintained in buffer [10 mM tris(hydroxymethyl)aminomethane pH 8, 1 mM NaCl, and 1 mM ethylenediaminetetraacetic acid (EDTA)] at a stock concentration of  $100 \mu\text{M}$  and was diluted to desired concentrations when required. Higher

saline concentrations (150 mM) were used when testing for Debye screening limited responses. Electrolytes containing NaCl,  $\text{MgCl}_2$ , and  $\text{Co}(\text{NH}_3)_6\text{Cl}_3$  salts (Sigma Aldrich) were made up to the desired dilution using Millipore de-ionized  $\text{H}_2\text{O}$ . When testing the role of multivalent ions during DNA hybridization, DNA was suspended in buffer without EDTA, just to avoid competition with multivalent ions. Ag/AgCl (Warner instruments, USA) pseudoreference electrodes were used. The wire surfaces were cleaned with sandpaper and chlorinated in bleach prior to every experiment. Experiments were performed in a light-tight environment. The different DNA strands were additionally used under identical conditions to ascertain the impedance dependence on molecular length before and after hybridization.

### B. Electrical instrumentation

CV measurements were performed using a Keithley 4200 semiconductor parameter analyzer. CV profiles were recorded at various small-signal frequencies. The reference electrode was supplied with an ac signal superimposed on a slow dc sweep, while the wafer chuck was used as ground. The transistor transfer characteristics [current-voltage ( $IV$ )

TABLE I. Various DNA strand sequences and associated lengths used for experimental runs.

Type	DNA sequence
B1 (16 bp ssDNA) probe	5'-GCTCAAAGTCTCGCAG-3'
B2 (16 bp ssDNA) target	5'-CTGCGAGACTTTGAGC-3'
C1 (25 bp ssDNA) probe	5'-GCATCTGGGCTATAAAAGGGCGTCG-3'
C2 (25 bp ssDNA) target	5'-CGACGCCCTTTTATAGCCCAGATGC-3'
D1 (48 bp ssDNA) probe	5'-GCATCTGGGCTATAAAAGGGCGTCGGTATCCAAGGTTCCGGATACGAG-3'
D2 (48 bp ssDNA) target	5'-CTCGTATCCGGAACCTTGGATACCGACGCCCTTTTATAGCCCAGATGC-3'

relationship, the drain current  $I_D$  vs the CG bias ( $V_{CG}$ ) were recorded using a Keithley 236 source measure unit for the drain ( $V_D = 1$  V) and a Keithley 2400 was used to sweep  $V_{CG}$ . Prior to adding DNA, the transconductance ( $g_m$ ) seen from both the CG and the SG was recorded in order to calibrate the capacitance ratio [18]. In addition to  $IV$  analysis, impedance measurements were performed by monitoring the small-signal transistor gain as a function of frequency as previously described [15,32]. Briefly, a single-toned sinusoid waveform was applied (Stanford Research Systems DS345, CA, USA) through the Ag/AgCl reference electrode, while the dc bias was supplied via the control gate independently (Keithley 2400, USA). The output current of the transistor was fed to a lock-in amplifier (LIA) (Stanford Research Systems, SR844, CA, USA) through a transimpedance amplifier (TIA) (SR 570, Stanford Research, USA). Bode responses and  $IV$  sweeps were measured intermittently to ascertain the operating point stability. The CG was then adaptively biased to maintain a constant operating point during the impedance measurement. Ultraviolet (UV) spectrophotometry (Shimadzu UV 3600, USA) was used to ascertain the absorbance of nonprecipitated DNA during multivalent ion treatment.

### C. Device operation

The CvMOS (Fig. 1) working principle is similar to what was previously outlined [15,18] in Parts I and II. The transistor was operated in both quasistatic and ac impedance mode. Briefly, the floating-gate potential ( $V_{FG}$ ) is perturbed by analyte adsorption on the SG surface. A change in  $V_{FG}$  directly affects the readout current:

$$I_D = \frac{\mu C_{\text{tun}} W}{2L} (V_{FG} - V_{\text{th,FG}})^2, \quad (4)$$

where  $I_D$  is the drain current in saturation,  $\mu$  is the mobility,  $C_{\text{tun}}$  is the tunnel oxide capacitance per unit area,  $W$  is the channel width,  $L$  is the length, and  $V_{\text{th,FG}}$  is the threshold voltage seen from the FG when  $I_D$  reaches  $1 \mu\text{A}$ .

A  $V_{CG}$  sweep is then performed to determine  $V_{\text{th,FG}}$  which is the threshold voltage seen from the CG. Threshold is defined at constant  $V_{FG}$ , which implies constant  $I_D$  from Eq. (4) for a given device.  $V_{FG}$  is related to  $V_{CG}$  by

$$V_{FG} = \frac{Q}{C_T} + \frac{C_{\text{gs}}}{C_T} V_S + \frac{C_{\text{gd}}}{C_T} V_D + \frac{C_{CG}}{C_T} V_{CG} + \frac{C_{SG}}{C_T} (\psi_O - V_{\text{ref}}), \quad (5)$$

where  $Q$  is the charge stored on the FG,  $C_{\text{gs}}$  is the gate-to-source capacitance,  $C_{\text{gd}}$  is the gate to drain capacitance,  $C_{CG}$

is the control gate interpoly oxide capacitance,  $C_{SG}$  is the sensing gate interpoly oxide capacitance, and  $C_T$  is the total capacitance seen by the FG and expressed by

$$C_T = \left( \frac{C_{\text{tun}} C_{\text{dep}}}{C_{\text{tun}} + C_{\text{dep}}} \right) + C_b + C_{\text{gs}} + C_{\text{gd}} + C_{CG} + C_{SG}. \quad (6)$$

Here  $C_{\text{dep}}$  is the depletion layer capacitance and  $C_b$  is the FG to bulk capacitance.  $V_{CG}$  is the voltage applied at the CG to bias the device, while  $V_{SG}$  is determined by  $\psi_O$  and  $V_{\text{ref}}$ . As highlighted previously [18],  $V_{CG}$  driven readout results in an amplified measure of  $\psi_O$  and the amplification factor  $A_C$  is primarily determined by the ratio between the two input capacitors  $C_{SG}$  and  $C_{CG}$ :

$$A_C = \frac{W_{SG} L_{SG} \epsilon_{\text{ox}} // C_{\text{dl}}}{W_{CG} L_{CG} \epsilon_{\text{ox}} t_{\text{ox}}}, \quad (7)$$

where  $W_{CG} L_{CG}$  and  $W_{SG} L_{SG}$  are the layout areas of the CG and SG, respectively,  $C_{\text{dl}}$  is the double layer capacitance, and  $t_{\text{ox}}$  is the tunnel oxide thickness. We can then state the threshold voltage shift observed from CG as

$$\Delta V_{\text{th,CG}} = \frac{-Q}{C_T} - \frac{C_{\text{gs}}}{C_T} V_S - \frac{C_{\text{gd}}}{C_T} V_D - A_C \Delta \psi_O. \quad (8)$$

It is also possible to use the CG to modulate the field in the SG control oxide, which can perturb  $\sigma_O$  and  $\psi_O$  [18], thus affecting DNA adhesion [15]. From Eq. (8), once  $\Delta V_{\text{th,CG}}$  is measured and with the value of  $A_C$  is known,  $\Delta \psi_O$  can be determined.

With frequency-mode operation and impedance analyses,  $V_{CG}$  or  $V_{\text{ref}}$  was first tuned to a desired dc value such that the drain current level was maintained in saturation at a predefined value usually set between 10 and 50  $\mu\text{A}$ . The drain bias was set to 1 V by the TIA. The output of the TIA was then fed to the LIA and the Bode response was recorded. Equation (9) expresses the TIA output [32,33]:

$$v_{\text{out}} = i_d R_D, \quad (9)$$

where  $R_D$  is the feedback resistance and  $v_{\text{out}}$  is the small-signal output of the TIA. In the saturation region of the transistor, the small-signal current  $i_d$  can be recast in the form of  $g_m v_{\text{gs}}$ , where  $v_{\text{gs}}$  is the small-signal gate-to-source voltage and  $g_m$  is the small-signal transconductance. The gate voltage can be represented in terms of the transfer function across the electrolyte and the DNA layer given by the relation  $v_{\text{gs}} = H(j\omega) v_{\text{in}}$  where  $v_{\text{in}}$  is the ac small signal delivered from the reference electrode. The transfer function across the DNA-transistor interface, neglecting the effect of source and drain

parasitics, can be expressed by

$$H(j\omega) = \frac{1 + sR_{\text{DNA}}C_{\text{DNA}}}{1 + s[R_{\text{sol}}C_{\text{ox}} + R_{\text{DNA}}(C_{\text{ox}} + C_{\text{DNA}})] + s^2R_{\text{DNA}}C_{\text{DNA}}R_{\text{sol}}C_{\text{ox}}}, \quad (10)$$

where  $C_{\text{OX}} = \frac{(C_{\text{tun}}+C_{\text{CG}})C_{\text{SG}}}{(C_{\text{tun}}+C_{\text{CG}})+C_{\text{SG}}}$  is the effective oxide capacitance. Here  $R_{\text{sol}}$  defines the solution resistance,  $s = j\omega$  from the Laplace transform, and  $C_{\text{DNA}}$  and  $R_{\text{DNA}}$  are the capacitance and resistance of the DNA membrane. Additional effects of the source and drain parasitic contact-lane capacitances  $C_{\text{line}}$  are not considered in the analytical derivation for simplicity [32]. To a first-order approximation, the dominant poles and zeros of the Bode response are given by

$$P_1 = \frac{1}{R_{\text{sol}}C_{\text{ox}} + R_{\text{DNA}}(C_{\text{ox}} + C_{\text{DNA}})}, \quad (11)$$

$$P_2 = \frac{1}{R_{\text{sol}}C_{\text{DNA}}} + \frac{1}{R_{\text{sol}}C_{\text{OX}}} + \frac{1}{R_{\text{DNA}}C_{\text{DNA}}}, \quad (12)$$

$$Z_1 = \frac{1}{R_{\text{DNA}}C_{\text{DNA}}}. \quad (13)$$

We immediately notice that if  $R_{\text{sol}}$  is low, which is an acceptable assumption when the background electrolyte salinity is high,  $P_1$  and  $Z_1$  essentially capture molecular relaxations within the bandwidth of the overall response.

### III. RESULTS AND DISCUSSION

#### A. Role of surface charges

CV measurements were performed on EOS capacitors as shown in Figs. 2(a) and 2(b). Two separate interfaces were studied. The first EOS capacitor had a traditional thermally grown  $\text{SiO}_2$  interface, while the other had a highly doped polysilicon surface on top of thermally grown  $\text{SiO}_2$ . The thickness of the thermal  $\text{SiO}_2$  in both cases was  $\sim 30$  nm. The latter was used to corroborate transistor measurements as it mimics the interface of the C $\nu$ MOS-electrolyte interface. Thermally grown  $\text{SiO}_2$  possesses an intrinsically high surface hydroxyl charge density [4] ( $\sim 10^{18}/\text{m}^2$ ) and exhibits a near Nernstian ( $\sim 48$  mV/pH) pH response. Low-pressure chemical vapor deposition polysilicon, however, has a hydrated native oxide, is slightly porous [34], possesses a moderate to low surface hydroxyl density, and exhibits a non-Nernstian pH response [18]. Hybridization measurements were performed on PLL-coated EOS capacitors and we found a clear difference in  $V_{\text{FB}}$  recorded between the two surfaces. While hybridization measurements on  $\text{SiO}_2$  surfaces resulted in a  $\Delta V_{\text{FB}}$  of  $\sim 18$  mV, measurements on polysilicon interfaces showed a  $\Delta V_{\text{FB}} \sim 50$ –60 mV. This clearly suggests that intrinsic charge screening due to exposed surface groups reduces the sensitivity. In a previous study we observed that when the bulk salinity changed from 1 mM to 150 mM,  $\Delta V_{\text{FB}}$  shifted from  $\sim 50$  mV to  $\sim 10$ –20 mV, clearly indicating Debye screening limited responses [35]. Collectively the above results suggest that intrinsic surface properties, bulk salinity, and the net density of exposed hydroxyl charges play critical roles in signal generation, screening, and sensitivity.

Next, in order to ascertain the effect of varying background  $\text{pH}_B$  on molecular charge sensitivity, we varied  $\text{pH}_B$  and measured  $\Delta\psi_O$  [Fig. 2(c)]. We observed that as  $\text{pH}_B$  increased from 5 to 9,  $\Delta\psi_O$  increased (plotted as  $\Delta\psi_{\text{hyb}}$ ) from  $\sim 20$  mV to  $\sim 85$  mV indicating an enhancement in sensitivity. We compared two independent models to experiments: (a) the PB approximation in which the DNA layer was assumed to be akin to a sheet charge [Eq. (2)] and (b) a membrane model in which the electrostatics between the SG and DNA was described using Eq. (14). We included the partition effect, where ( $\Delta G_m$ ) represents the energy barriers that ions encounter due to permittivity differences between the membrane and electrolyte phase [Eq. (15)] [11],  $a$  is the ion radius, and  $z$  is the valency.

$$E \frac{dE}{d\psi} = \frac{2en_O}{\epsilon_{\text{eff}}} \sinh\left(\frac{\Delta G_m + e\psi}{kT}\right), \quad (14)$$

$$\Delta G_m = -\frac{69z^2}{a} \left(\frac{1}{\epsilon_{\text{eff}}} - \frac{1}{\epsilon_{\text{medium}}}\right)^* 0.01036 \text{ eV}. \quad (15)$$

Here  $\epsilon_{\text{eff}}$  represents the permittivity in the DNA layer and  $\epsilon_{\text{medium}}$  signifies the permittivity in the bulk electrolyte. This energy difference stems from the Born charge-dielectric interaction [11,15,36] in which the self-energy of the ion undergoes a penalty when it crosses over from a medium of high permittivity to that of low permittivity. In order for the overall  $\Delta G_m$  to be negative, ions permeate into a medium of higher permittivity (i.e., in water,  $\epsilon_{\text{medium}} = 80$ ) and incur an energy cost if present in a medium of lower permittivity (i.e., tightly packed DNA layers). This enhanced energy penalty leads to a lower screening charge [16] within the DNA layer which directly influences the overall  $\Delta\psi_O$ . A detailed analysis of the simulation methodology was presented in part II [15].

As shown in Fig. 2(c), we found the best fit across the  $\text{pH}_B$  range to occur when ions were completely excluded from the DNA layer and  $\epsilon_{\text{eff}}$  was reduced leading to a large negative  $\Delta G_m$ . With ions present, the extra screening from ions prevented a clear fit around  $\text{pH}_B = 9$ . The PB approximation on the contrary failed to corroborate experiment across the entire  $\text{pH}_B$  range except at  $\text{pH}_B = 5$ , clearly indicating the limitation of the model at higher  $\text{pH}_B$ . In short, signal generation during DNA hybridization is affected by surface hydroxyl screening and membrane screening, but the question remains as to why we observed such a trend in  $\Delta\psi_O$  when  $\text{pH}_B$  was varied.

In order to corroborate this trend we first revisit the results by Zhang *et al.* [21]. The authors showed that during hybridization, single-stranded DNA (ssDNA) was indeed more effectively screened at lower  $\text{pH}_B$ , which then led to an increase in the hybridization efficiency, revealed by mechanical deflections of a nanocantilever. If this were true in our case, one would expect to observe the opposite trend in  $\Delta\psi_O$  (i.e., largest magnitude of  $\Delta\psi_O$  at  $\text{pH}_B = 5$ ). In addition, DNA hybridization performed at two different  $\text{pH}_B$

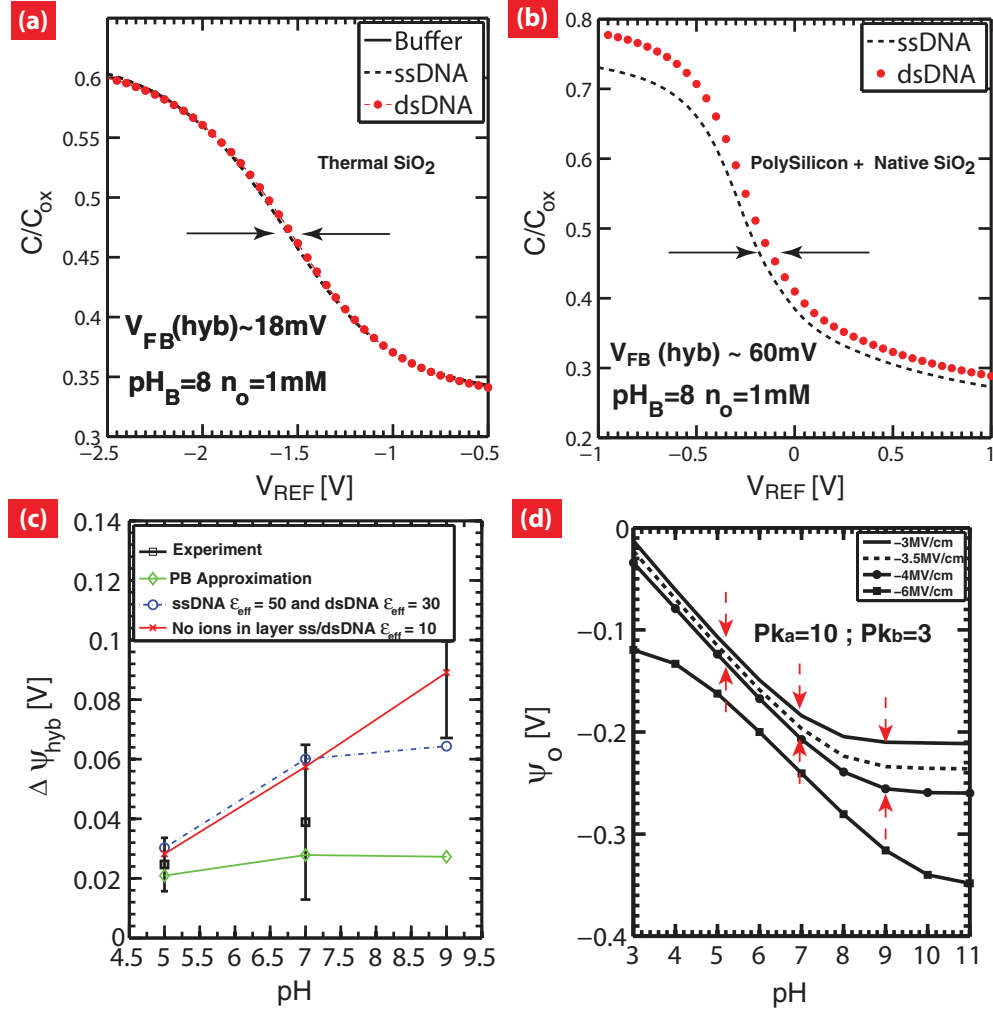


FIG. 2. (Color online) Experimental CV analyses of DNA hybridization performed on PLL-coated EOS capacitors, depicting  $V_{FB}$  shifts for (a) SiO<sub>2</sub> interface and (b) polysilicon interface.  $V_{FB}$  shifts of  $\sim 18$  and  $\sim 60$  mV are observed, respectively, indicating the role of surface buffering in signal generation. (c) Effect of varying background pH on the DNA hybridization signal using the  $C_V$ MOS transistors. As the pH is increased from 5 to 9, the hybridization signal ( $\Delta\psi_O$ ) increased. The best theoretical fit to experiment occurs when a membrane model is assumed, where ions are completely excluded from the membrane and the permittivity within the DNA layer is low ( $\sim 10$ ). The PB model in comparison fails to provide an explanation of the experimental observation. (d) Simulation when a negative  $E$  field is applied at the SG interface, where the pH insensitive region shifts to higher pH values. Any further change in  $E$  field induces a maximal change in  $\psi_O$  within the pH insensitive region (starting at pH 9), which is the region of lowest buffering. As pH reduces towards 5, the  $\psi_O$  response to pH becomes more linear, which is the region of strong buffering. This shows that in addition to membrane permittivity, which decides the overall net magnitude, the effect of the DNA charges on the surface chemical equilibrium dictates the maximal hybridization sensitivity.

conditions did not show a significant difference in interface impedance (described in Sec. III D), which indicated that  $pH_B$  induced screening of DNA was not a dominant factor in signal generation at the transistor interface and that factors other than proton screening were involved.

Recent work has shown that the ionization properties of the interface can be modulated by the application of an  $E$  field [18,27]. DNA is negatively charged and when immobilized on the SG surface is akin to applying a net negative field at the interface. We simulated  $\psi_O$  vs  $pH_B$  under the influence of a negative  $E$  field [Fig. 2(d)], following the approach outlined in Part I [18]. Briefly, the fits from  $pK_a = 10$  and  $pK_b = 5$  represent equilibrium conditions for an EOS capacitor with a native polysilicon interface. Equations (16)–(18) were self-consistently solved under varying  $E$ -field conditions in

the underlying oxide.

$$\sigma_O = e\Gamma_{OH} \left[ \frac{H_S^+}{K_b} - \frac{K_a}{H_S^+} \right]. \quad (16)$$

Here  $H_S^+$  is the surface proton concentration,  $\Gamma_{OH}$  represents the neutral site density, and  $K_a$  and  $K_b$  represent the association and dissociation constant. The surface proton concentration is then related to the bulk proton concentration  $H_B^+$  through the Boltzmann relationship outlined in the following equation:

$$H_S^+ = H_B^+ \exp\left(\frac{-e(\psi_O - V_{ref})}{kT}\right). \quad (17)$$

The  $E$  field in the underlying oxide must then balance both the surface and double layer charge through Eq. (18), where  $\sigma_{dl}$

represents the double layer charge (see Part I for details) [18].

$$E_{ox} = -\frac{(\sigma_o + \sigma_{dl})}{\epsilon_{ox}}. \quad (18)$$

We found that under the influence of negative  $E$  fields the  $pH$  insensitive region shifted to higher  $pH_B$  values, while the slope of the  $pH$  response exhibited a near Nernstian response at low to medium  $pH_B$ . When we doubled the applied  $E$  field (i.e., akin to doubling the DNA charge) we noticed that the maximal difference in  $\psi_O$  (indicated by the arrows and implying surface potential variations during hybridization) occurred at  $pH_B = 9$  (where the  $pH$  response is flat and least sensitive) and gradually decreased towards  $pH_B = 5$  (where the  $pH$  response is most sensitive). This indicated that through a combination of  $E$  field (i.e., due to DNA charges), choice of surface equilibrium constants, and  $pH_B$  (i.e., a chemical bias), the interface was pushed into a  $pH$  insensitive region ( $pH_B = 9$ ). At this  $pH$  condition the surface buffering capacity is weak and screening of molecular charges is low. We point out that this  $pH_B$  insensitive region is not the point of zero charge (PZC). When

we simulated the effect of applying an even higher hypothetical negative  $E$  field of  $-6$  MV/cm, which is exactly double the field of ssDNA ( $-3$  MV/cm), we noticed that the trend began to reverse (i.e.,  $\Delta\psi_O$  at  $pH_B = 5$  appeared larger). The above results suggest that surface buffering, membrane screening, and the  $E$ -field dependence of surface ionization together determine the  $\psi_O$  response during DNA hybridization.

### B. Effect of surface modification

Prior to DNA immobilization the chips were coated with PLL in order to guarantee electrostatic interaction between DNA and the surface, and negate some of the native hydroxyl charge. As mentioned earlier, it is important to know the operating point along the  $pH$  response curve in order to completely corroborate experimental data. With surface coatings, the slope of the response curve can change [37]. Following the method outlined in [37], we simulated the effect of adding a surface coating with different surface ionization constants and site densities [Fig. 3(a)]. In addition to the native surface

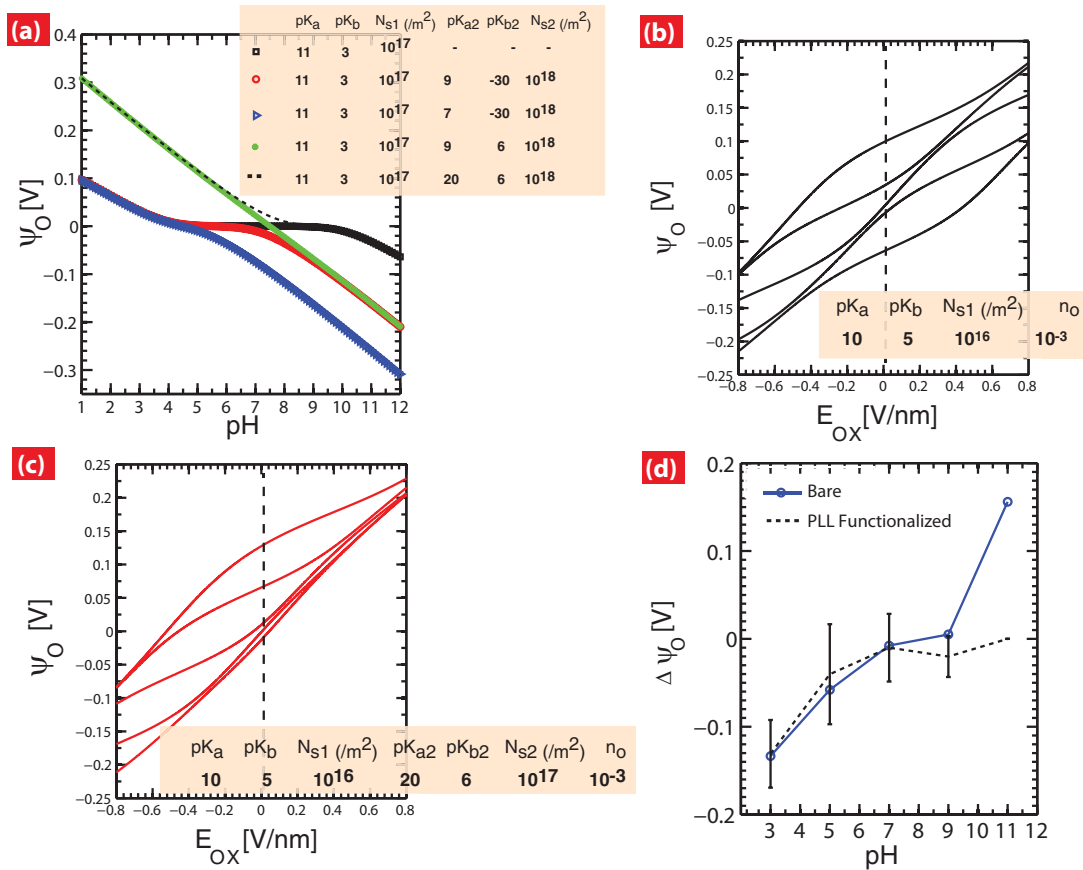


FIG. 3. (Color online) (a) Variation in  $\psi_O$  as a function of  $pH_B$  for variations in  $\Delta pK_2$ ,  $N_{s1}$ , and  $N_{s2}$ . Decreasing  $pK_{b2}$  from  $-30$  to  $6$  improves the slope of the  $pH$  response at lower  $pH$  values, while decreasing  $pK_{a2}$  from  $9$  to  $7$  improves the slope at higher  $pH$  values. Increasing  $pK_{a2}$  to  $20$  pushes the  $pH$  insensitive region to higher  $pH_B$  values. (b)  $\psi_O$  vs  $E_{ox}$  for varying  $pH_B$  from  $11$  to  $3$  (bottom to top). When  $pH_B$  is in the range between the  $2pK$ 's, the surface buffering is weak with  $pH_{PZC} \sim 7$ . Here  $pK_a = 10$  and  $pK_b = 5$ . The dotted line represents the  $E_{ox}$  applicable during readout. (c)  $\psi_O$  vs  $E_{ox}$  for varying  $pH_B$  from  $11$  to  $3$  (bottom to top) with a PLL layer present. Surface ionization parameters are listed in the figure. Notice how the  $pH$  response reduces at high  $pH_B$  values. The surface buffering effect is also more pronounced (slope is smaller) for a broader range of  $pH_B$  values as seen between  $-0.2$  and  $+0.2$  V/nm. Here  $pK_{a2} = 20$  and  $pK_{b2} = 6$  is an approximation for PLL. The dotted line represents the  $E_{ox}$  applicable during readout. (d) Experimental observation of  $\psi_O$  vs  $pH_B$  for surface with and without the PLL coating. Notice the reduction in the  $pH_B$  response at higher  $pH_B$  values agrees with the simulations shown in (a) and (c). Error bars represent an average of three experimental observations.

properties, namely,  $pK_a = 11$ ,  $pK_b = 3$ , and  $N_S = 10^{17} \text{ m}^{-2}$ , the surface coating was described by a similar  $2 - pK$  model by  $pK_{a2}$ ,  $pK_{b2}$  and  $N_{S2}$ . The new  $\sigma_O$  condition is given by Eq. (19). The interface  $E$ -field dependent ionizability was then simulated in a similar fashion as previously described for a generic surface.

$$\sigma_O = e \left\{ \Gamma_{OH} \left[ \frac{H_S^+}{K_b} - \frac{K_a}{H_S^+} \right] + \Gamma_{OH2} \left[ \frac{H_S^+}{K_{b2}} - \frac{K_{a2}}{H_S^+} \right] \right\}. \quad (19)$$

Assumptions made in this theoretical model were as follows: (i) thickness of the coating was not considered and (ii) both the native interface and surface coating shared the same plane but were described by different surface constants and site densities. We immediately noticed that addition of a surface coating influences the  $pH$  response drastically. Decreasing  $pK_{a2}$  improved the  $pH$  response at high  $pH_B$ , while increasing  $pK_{b2}$  did the same for the acidic branch. When we simulated the system with approximate  $pK_{a2}$  and  $pK_{b2}$  values for PLL (20 and 6, respectively) with a PZC around 12 [38], we found that the  $pH$  insensitive region extended into the basic branch. This signified the need to ascertain the role of surface coatings *a priori* since the overall  $pH$  sensitivity could shift either way between non-Nernstian and Nernstian responses, which could have a strong effect on hybridization sensitivity. In Fig. 3(b) we studied the effect of modulating the underlying  $E$  field as a function of  $pH_B$  on an EOS system and plotted the resulting  $\psi_O$ . As the electric field was swept from  $-0.8 \text{ V/nm}$  to  $+0.8 \text{ V/nm}$ , intrinsic hydroxyl charges began to ionize in response to the applied field. The surface properties described a non-Nernstian  $pH_B$  response with the region in-between the two  $pK$ 's exhibiting a poor buffering effect (i.e., lowest ionizable hydroxyl charge and hence lowest  $pH_B$  sensitivity). With the application of a PLL coating [Fig. 3(c)] we found that the buffering effect improves across the low to medium  $pH_B$  range since the  $pH$  insensitive region shifted to higher  $pH_B$ . Experimental observations [Fig. 3(d)] on the CMOS depict the  $pH_B$  sensitivity before and after PLL addition. We immediately noticed that the difference in  $\psi_O$  reduced drastically at high  $pH_B$ , while it maintained a near Nernstian response at low  $pH_B$ . Since the maximal DNA hybridization sensitivity was observed at  $pH_B = 9$  and sensitivity is maximal when the  $pH$  response is least sensitive, the additional effect imparted by the PLL coating most likely played a key role in establishing this condition.

### C. The response curve

It is critical to model the relation between complementary DNA strands in solution ( $N_C$ ) and the maximal density of surface-bound double-stranded DNA ( $N_{ds}$ ) for hybridization sensing. In Fig. 4 we depict the effect of varying the target concentration  $N_C$  on the net signal sensitivity. We fitted the experimental data points to two separate adsorption isotherms of Langmuir and Langmuir-Freundlich (LF) approximations. The Langmuir isotherm is based on the assumption of a monolayer molecular coverage without biomolecular interaction or

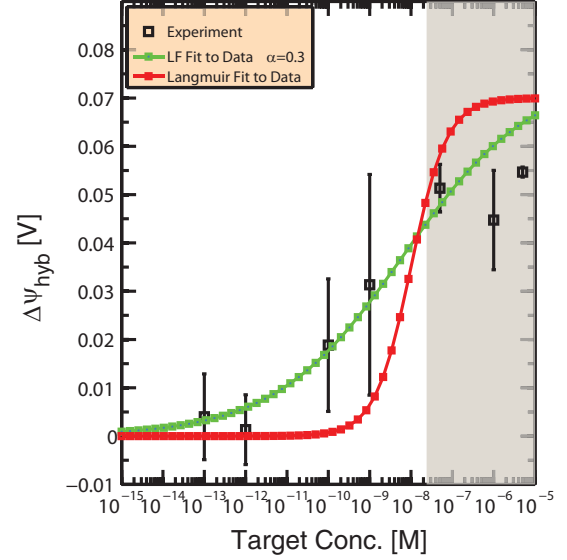


FIG. 4. (Color online) Simulated and measured titration response curves. Langmuir and Langmuir-Freundlich (LF) isotherms are used to fit the experimental data:  $\alpha = 1$  for the Langmuir isotherm and  $\alpha = 0.3$  for the LF isotherm, which accounts for surface heterogeneity. At high target concentrations the response first saturates and then decreases slightly indicating Coulomb blockage of DNA hybridization. A limit of detection between  $\sim 0.1$ – $1 \text{ nM}$  and  $k_D \sim 20 \text{ nM}$  is extracted.

surface heterogeneity as shown below [11,25]:

$$N_{ds} = N_P \frac{N_C K_A}{N_C K_A + 1}, \quad (20)$$

where  $N_P$  represents the total surface-bound single-stranded DNA (ssDNA) and  $K_A$  is the equilibrium association constant. However, since the transistor measures charge, Eq. (20) can be recast into the form [25,39]

$$\Delta V_{th} = \frac{q}{C_O} [B]_{\max} \frac{N_C K_A}{N_C K_A + 1}. \quad (21)$$

Here  $q$  is the charge contributed by the adsorbed molecules,  $C_O$  is the molecule to channel capacitance coupling, and  $[B]_{\max}$  is the maximal density of functional binding sites.  $\frac{q}{C_O} [B]_{\max}$  and  $K_A$  represent the maximal sensors response and affinity properties [25], which can be extracted from experiments for a series of  $N_C$ . Most interfaces, especially complementary metal-oxide semiconductor (CMOS) postprocessed surfaces, exhibit a large degree of heterogeneity. In addition, given the purely electrostatic DNA-PLL interaction, the uniformity in surface binding energies and the assumption of no intermolecular interaction has limited applicability. In order to account for such effects, various extensions to the Langmuir isotherm have been proposed. One such model is the LF isotherm outlined as follows [11]:

$$\Delta V_{th} = \frac{q}{C_O} [B]_{\max} \frac{(N_C K_A)^\alpha}{(N_C K_A)^\alpha + 1}, \quad (22)$$

where  $\alpha$  is a parameter between 0 and 1 to account for the surface heterogeneity. When  $\alpha = 1$ , the LF isotherm reduces to the Langmuir isotherm. As shown in Fig. 4, the LF isotherm provided a reasonable fit to the data with  $\alpha = 0.3$ , while the

generic Langmuir isotherm failed to provide a good match. From the LF fit we extracted a limit of detection between 0.1 and 1 nM and an association constant  $K_A$  of  $0.5 \times 10^8 (M^{-1})$  ( $K_D \sim 20$  nM and  $K_A = 1/K_D$ ). Remarkably this value of  $K_D$  (dissociation constant) is lower than the one reported on lysine-coated nanowires ( $K_D \sim 200$  nM) [3], larger than the values reported on PNA-DNA interaction on nanowire FETs ( $K_D \sim 5$  nM) [40], but in line with simulation results presented in [11] ( $K_D \sim 10$  nM). We attribute these differences to surface heterogeneity, the choice of  $\alpha$  in the LF isotherm, and the low intrinsic surface charge density exhibited by polysilicon surfaces. We also point out that at high target concentrations, the  $\Delta\psi_O$  saturated and even reduced slightly. We attribute this reduction in sensitivity to Coulomb blockage of DNA hybridization [24], in which incoming complementary DNA strands feel repulsion upon entry into the probe layer. These results strongly suggest that surface heterogeneity, probe concentrations and target concentrations should be considered in order to fully explain the surface response [41] and should be carefully tailored to maximize sensitivity.

#### D. Mechanisms of signal enhancement

It is well known that in order to achieve efficient hybridization and reduce interstrand repulsion, the background saline concentration needs to be high [26]. However, as the saline concentration increases, Debye screening limits the net molecular charge detectable at the transistor interface. Such screening limited responses make it hard to detect and sort different lengths of DNA molecules. It is for this very reason that most hybridization sensing experiments are performed under low saline conditions. We used frequency-mode Bode plots (see methods) in which the poles and zeros are sensitive to molecule-electrode interactions to detect DNA hybridization as a function of molecular length (Fig. 5). We plot the *ex situ* transfer function (background buffer subtracted) in Figs. 5(a) and 5(b). We observed that as the molecular length increased from 16 to 48 base pairs

(bp), the interfacial impedance increased as evidenced by the attenuation in magnitude [Fig. 5(a)] and the position of the trough. The phase plot depicted a corresponding decrease typical of an RC relaxation with the trough moving towards lower frequencies as molecular length increased. The RC time constant is sensitive to both the interfacial resistance and a large induced interfacial dipole moment, a consequence of increased molecular weight of the adsorbed DNA. Counterion relaxation is also known to occur in the range between 100 Hz and 100 KHz and induce a rotational time constant dependent on molecular weight as well [42]. Together these effects give rise to a change in the net interfacial impedance. We also point out that the SG size is large, which leads to a large double layer capacitance. As the frequency is swept, the double layer polarization rolls off immediately within a few KHz and thus polarization limitations are avoided at higher frequencies.

While frequency-mode detection avoids limitation due to Debye screening, allows for biosensing under high saline conditions, and is pH insensitive [Figs. 6(a) and 6(b)], direct detection of intrinsic molecular charge is hard. So the question remains as to whether it is possible to improve the hybridization response and at the same time preserve the ability to detect charge. We examined the effect of adding trace amounts of multivalent salt to a low monovalent saline background during the hybridization phase alone and measured  $\Delta\psi_O$  (Fig. 7). Immobilization of ssDNA was carried out in 1 mM NaCl, while complementary ssDNA was added in 1 mM NaCl solution with trace  $MgCl_2$  and  $Co(NH_3)_6Cl_3$  ranging from 1 to 100  $\mu M$ . It was immediately clear that adding trace amounts of multivalent ions improved the surface sensitivity by nearly  $\sim 80$ –100 mV with 100  $\mu M$  of  $MgCl_2$  and  $\sim 60$  mV with just 10  $\mu M$  of  $Co(NH_3)_6Cl_3$ . Any further increase in the  $Co(NH_3)_6Cl_3$  concentration led to a reversal in  $\psi_O$  (not shown), indicating overscreening and possible charge inversion at the transistor surface [18]. We explain the increased sensitivity as follows. As multivalent ions are introduced into the sample solution, the

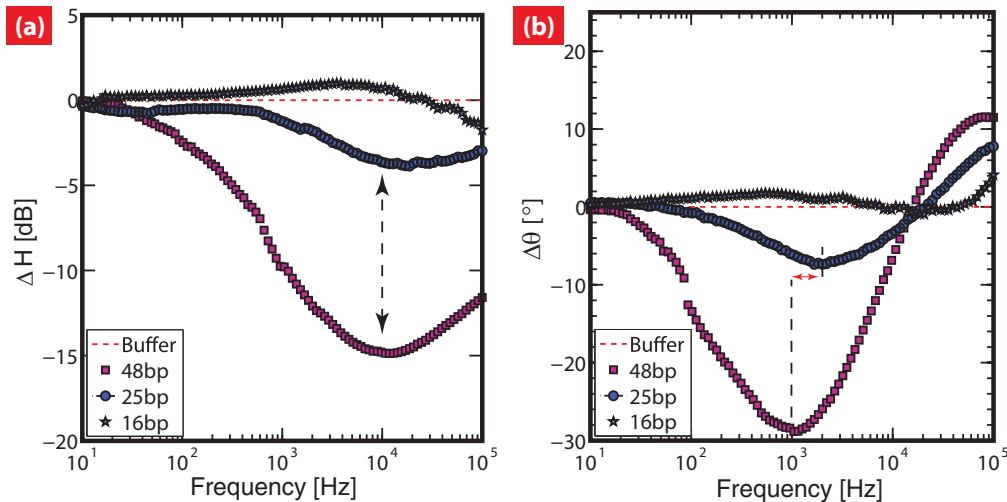


FIG. 5. (Color online) *Ex situ* frequency response depicting (a) magnitude and (b) phase for short stranded DNA hybridization as a function of varying nucleic acid length. As the length of the DNA strand is increased, the interfacial impedance increases (shown by the dashed arrow) leading to a larger attenuation in the magnitude plot. A corresponding relaxation is observed in the phase. An increase in the RC time constant is depicted by the red arrow.

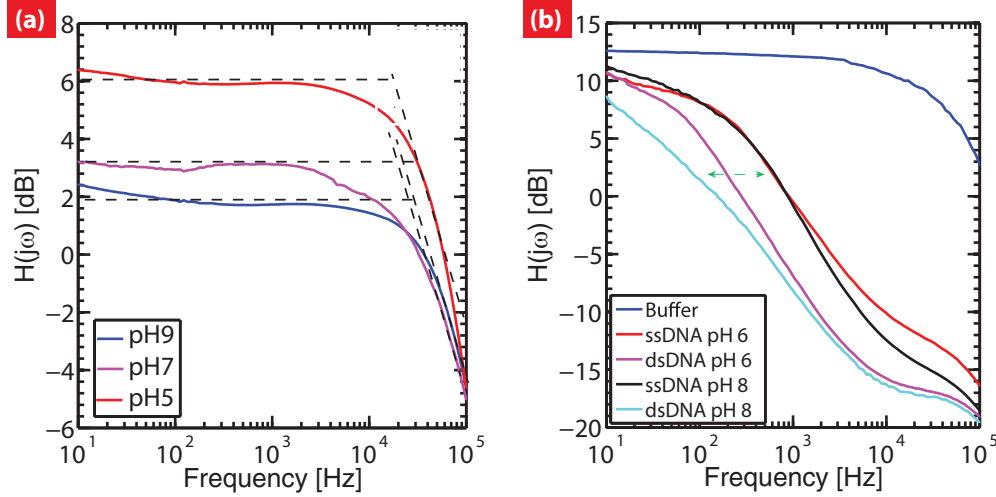


FIG. 6. (Color online) (a) Bode responses performed under different  $pH_B$  conditions. Notice how the pole ( $P_2$ ) (the only pole in the system without the DNA molecule) does not shift with varying bulk  $pH_B$  indicative of  $pH_B$  insensitivity. (b) DNA hybridization under different  $pH_B$  conditions. The increase in capacitance upon complimentary strand addition is similar, although a slight increase in interfacial resistance at  $pH_B = 8$  is observed. This increase in resistance is within the error bar in this frequency mode of operation (not shown).

counterion cloud around DNA is perturbed [43]. Multivalent ions have a strong tendency to bind to DNA strands, displace monovalent ions [43], condense onto the phosphate backbone [30], and in some cases even reverse the charge on the molecule [44]. These previous studies suggested that the local screening cloud around the DNA molecule was predominantly comprised of trace multivalent ions, possibly due to enhanced electrostatic effects [44,45]. For example, a  $1 \mu\text{M}$  DNA and  $10 \mu\text{M}$   $\text{Co}(\text{NH}_3)_6\text{Cl}_3$  concentration in a sample would imply 10 Co ions for every ssDNA molecule. Given the DNA length to be  $\sim 25$  bp (i.e., 25 electrons for ssDNA and 50 electrons after duplex formation), would imply that the ssDNA molecule is almost completely screened when added to the chip in multivalent saline background. This in itself will allow for enhanced screening during the hybridization process. If the counterions were still strongly attracted to the DNA molecule, the screening would be higher and we would have observed a diminished  $\Delta\psi_0$  response. We, however, reiterate that once hybridization occurs, ions are excluded from the membrane owing to the low permittivity as previously explained. With multivalent ions the exclusion effect is stronger [Eq. (15)], since  $\Delta G_m$  is directly proportional to the square of valency. This causes ion exclusion from within the DNA layer and the multivalent ions form the screening layer just outside the DNA lattice. However, multivalent ions are in trace quantity, which implies a larger Debye length [Eq. (3)] and lower screening capacitance [46] which would directly induce an increase in  $\Delta\psi_0$ . We do point out that when we increased the background monovalent concentration to 100 mM, we did not observe any enhancement in signal upon multivalent ion addition (not shown), indicating that competition between monovalent and multivalent species is central to signal enhancement. In order to be certain that DNA did not completely precipitate out of solution under the influence of multivalent ions, we performed UV spectrophotometry studies under varying conditions of background trivalent salt [Fig. 7(b)]. We found that when  $\text{Co}(\text{NH}_3)_6\text{Cl}_3$  concentrations on the order of  $\sim 1$  mM were added, a lowering in the absorbance was observed. However,

at  $50 \mu\text{M}$  of  $\text{Co}(\text{NH}_3)_6\text{Cl}_3$  the amount of DNA precipitating out of solution was negligible, clearly showing that DNA precipitation during experiment was insignificant under the concentrations used.

Taken together, Figs. 7(a) and 7(b) suggest that multivalent ions condense onto DNA, cause aggregation, and induce condensation onto the sensing gate surface, thus improving the hybridization sensitivity and increasing the sensitivity to net molecular charge. In order to further corroborate the increase in interfacial DNA adsorption, we performed frequency-mode detection during the hybridization process [Figs. 7(c) and 7(d)] and found a clear increase in interfacial impedance with a  $RC$  relaxation occurring at  $\sim 1$  KHz. In comparison, hybridization measurements performed on 25 bp DNA in the absence of added multivalent ions showed a  $RC$  relaxation at  $\sim 3$  KHz (Fig. 5), which suggests that multivalent ions increase DNA aggregation at the interface. Impedance analysis under higher concentrations of  $\text{Co}(\text{NH}_3)_6\text{Cl}_3$  revealed an outward movement in the pole-zero response, indicating a reduced interfacial impedance possibly as a result of DNA desorption due to excessive ion condensation (not shown). It is interesting to note that in Fig. 7(d) we observed a slight decrease in the  $RC$  time constant with respect to the ssDNA, possibly due to trace Co ions within the DNA layers decreasing the ac resistance at the interface. Together these results suggest that modifying the local screening profile, inducing aggregation, and reducing repulsion by the addition of trace multivalent ions could be used as a signal enhancement strategy.

#### IV. CONCLUDING REMARKS

We presented detection of DNA hybridization using EOS capacitors and floating-gate ISFETs. We highlighted the roles of bulk  $pH$ , surface ionizability, surface coatings, and target concentration on signal generation. Our results suggest that in addition to surface properties, membrane screening and field-dependent surface ionization play key roles in deciding signal sensitivity. Models including permittivity differences

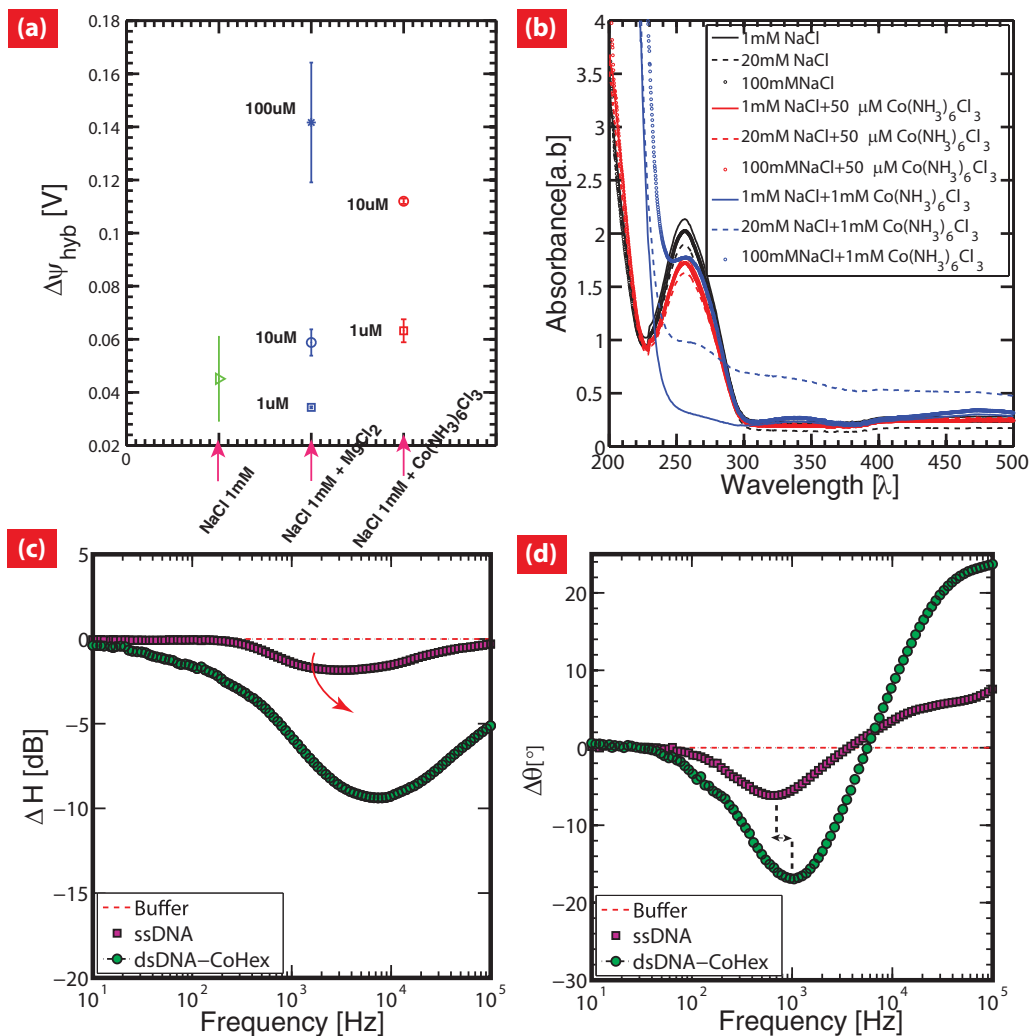


FIG. 7. (Color online) (a) Effect of adding trace amounts of multivalent ions to the complementary strands during hybridization. As the valency is increased,  $\Delta\psi_{\text{hyb}}$  sensitivity improves. (b) UV spectrophotometry measurements of 25 bp DNA treated with multivalent ions indicates no molecular precipitation when  $50 \mu\text{M}$   $\text{Co}(\text{NH}_3)_6\text{Cl}_3$  is added but strong precipitation for  $1 \text{ mM}$   $\text{Co}(\text{NH}_3)_6\text{Cl}_3$ . *Ex situ* impedance response depicting (c) magnitude and (d) phase for a hybridization reaction with trivalent ions added only during complementary strand addition. Notice a clear increase in interfacial resistance indicated by the large attenuation in signal when the complementary strand is introduced. A corresponding relaxation in phase is observed. The  $RC$  time constant decreases upon complementary strand addition in comparison to ssDNA [depicted by the arrow in (d)] indicating a slight reduction in interfacial resistance.

between the DNA layer and bulk were presented and fitted to experiments. Signal enhancement strategies using frequency-mode sensing and use of multivalent salts to perturb the local screening profile were proposed. DNA length sorting and signal enhancement by  $\sim 100 \text{ mV}$  was demonstrated.

#### ACKNOWLEDGMENTS

This work was supported by NSF MRSEC Grant No. DMR-0520404 through Cornell Center for Materials

Research (CCMR) Interdisciplinary Research Group (IRG). We would like to thank Professor Lois Pollack for assistance and guidance throughout the course of this study. We acknowledge the Nano Biotechnology Center (NBTC) at Cornell and the Cornell Nano-Scale Facility (CNF) for technical support. K.J. would like to thank Lihua Wang and Suzette A. Pabit for help with DNA and electrolyte preparation and Mark Hartman from Professor Dan Luo's group for assistance with UV spectrophotometry.

- [1] L. Bandiera, G. Cellere, S. Cagnin, A. De Toni, E. Zanoni, G. Lanfranchi, and L. Lorenzelli, *Biosens. Bioelectron.* **22**, 2108 (2007).  
 [2] M. Barbaro, A. Bonfiglio, and L. Raffo, *IEEE Trans. Electron Devices* **53**, 158 (2006).

- [3] Y. L. Bunimovich, Y. S. Shin, W.-S. Yeo, M. Amori, G. Kwong, and J. R. Heath, *J. Am. Chem. Soc.* **128**, 16323 (2006).  
 [4] J. Fritz *et al.*, *Proc. Natl. Acad. Sci. USA* **99**, 14142 (2002).  
 [5] G. Zheng *et al.*, *Nat. Biotech.* **23**, 1294 (2005).  
 [6] E. Katz and I. Willner, *Electroanalysis* **15**, 913 (2003).

- [7] E. Stern *et al.*, *Nature (London)* **445**, 519 (2007).
- [8] F. Uslu *et al.*, *Biosens. Bioelectron.* **19**, 1723 (2004).
- [9] A. Poghossian *et al.*, *Sens. Actuators B* **111–112**, 470 (2005).
- [10] I. Y. Wong and N. A. Melosh, *Biophys. J.* **98**, 2954 (2010).
- [11] Y. Liu and R. W. Dutton, *J. Appl. Phys.* **106**, 014701 (2009).
- [12] D. Landheer *et al.*, *J. Appl. Phys.* **98**, 044701 (2005).
- [13] D. Landheer *et al.*, *IEEE Sens. J.* **7**, 1233 (2007).
- [14] A. G. Cherstvy, *Biosens. Bioelectron.* **46**, 162 (2013).
- [15] K. Jayant, K. Auluck, M. Funke, S. Anwar, J. B. Phelps, P. H. Gordon, S. R. Rajwade, and E. C. Kan, *Phys. Rev. E* **88**, 012802 (2013).
- [16] T. Windbacher, V. Sverdlov, and S. Selberherr, in *Proceedings of 13th International Workshop on Computational Electronics, IWCE 2009, Beijing, 2009* (IEEE, Piscataway, NJ, 2009), p. 1.
- [17] M. W. Shinwari and M. J. Deen, *Sens. Actuators B* **171–172**, 463 (2012).
- [18] K. Jayant, K. Auluck, M. Funke, S. Anwar, J. B. Phelps, P. H. Gordon, S. R. Rajwade, and E. C. Kan, *Phys. Rev. E* **88**, 012801 (2013).
- [19] R. B. M. Schasfoort *et al.*, *Anal. Chim. Acta* **238**, 323 (1990).
- [20] G. Shalev, Y. Rosenwaks, and I. Levy, *Biosens. Bioelectron.* **31**, 510 (2012).
- [21] J. Zhang *et al.*, *Langmuir* **28**, 6494 (2012).
- [22] D. A. Cherepanov *et al.*, *Biophys. J.* **85**, 1307 (2003).
- [23] B. Dorvel, B. Reddy, and R. Bashir, *Anal. Chem.* **85**, 9493 (2013).
- [24] A. Vainrub and B. M. Pettitt, *Phys. Rev. E* **66**, 041905 (2002).
- [25] X. Duan *et al.*, *Nat. Nanotechnol.* **7**, 401 (2012).
- [26] C. Gentil, G. Philippin, and U. Bockelmann, *Phys. Rev. E* **75**, 011926 (2007).
- [27] Z. Jiang and D. Stein, *Langmuir* **26**, 8161 (2010).
- [28] C. Toumazou *et al.*, *Nat. Methods* **10**, 641 (2013).
- [29] B. Veigas *et al.*, *Biosens. Bioelectron.* **52**, 50 (2014).
- [30] V. A. Bloomfield, *Curr. Opin. Struct. Biol.* **6**, 334 (1996).
- [31] N. Y.-M. Shen, Z. Liu, C. Lee, B. A. Minch, and E. C.-C. Kan, *IEEE Trans. Electron Devices* **50**, 2171 (2003).
- [32] S. Ingebrandt *et al.*, *Biosens. Bioelectron.* **22**, 2834 (2007).
- [33] M. M. G. Antonisse *et al.*, *Anal. Chem.* **72**, 343 (1999).
- [34] N. Zehfroosh, M. Shahmohammadi, and S. Mohajezadeh, *IEEE Electron Device Lett.* **31**, 1056 (2010).
- [35] K. Jayant, K. Auluck, and E. C. Kan, in *Proceedings of IEEE Sensors Conference, Baltimore, Maryland, 2013* (IEEE, Piscataway, NJ, 2013), p. 1.
- [36] J. Israelachvilli, *Intermolecular and Surface Forces* (Academic Press, London, 1992).
- [37] A. van den Berg *et al.*, *Sens. Actuators* **8**, 129 (1985).
- [38] D. Stein, M. Kruithof, and C. Dekker, *Phys. Rev. Lett.* **93**, 035901 (2004).
- [39] M. Abe *et al.*, *J. Phys. Chem. C* **111**, 8667 (2007).
- [40] A. De *et al.*, *ACS Appl. Mater. Interfaces* **5**, 4607 (2013).
- [41] A. W. Peterson, R. J. Heaton, and R. M. Georgiadis, *Nucleic Acids Res.* **29**, 5163 (2001).
- [42] R. Pethig and D. B. Kell, *Phys. Med. Biol.* **32**, 933 (1987).
- [43] K. Andresen *et al.*, *Biophys. J.* **95**, 287 (2008).
- [44] A. Y. Grosberg, T. T. Nguyen, and B. I. Shklovskii, *Rev. Mod. Phys.* **74**, 329 (2002).
- [45] F. H. J. van der Heyden, D. Stein, K. Besteman, S. G. Lemay, and C. Dekker, *Phys. Rev. Lett.* **96**, 224502 (2006).
- [46] B. D. Storey and M. Z. Bazant, *Phys. Rev. E* **86**, 056303 (2012).